Development of a high-spectral-resolution lidar for continuous observation of aerosols in South America

Yoshitaka Jin*[a], Nobuo Sugimoto[a], Tomoaki Nishizawa[a], Pablo Ristori[b], Sebastian Papandrea[b], Lidia Otero[b], Eduardo Quel[b], and Akira Mizuno[c]
[a]National Institute for Environmental Studies, 16-2 Onogawa, Tsukuba, Japan;
[b]Centro de Investigaciones en Láseres y Aplicaciones, Juan Bautista de La Salle 4397—B1603ALO Villa Martelli, Buenos Aires, Argentina;
[c]Nagoya University, Furo-cho, Nagoya, Japan

ABSTRACT

Continuous monitoring of aerosol profiles using lidar is helpful for a quasi-real-time indication of aerosol concentration. For instance, volcanic ash concentration and its height distribution are essential information for plane flights. Depolarization ratio and multi-wavelength measurements are useful for characterizing aerosol types such as volcanic ash, smoke, dust, sea-salt, and air pollution aerosols. High spectral resolution lidar (HSRL) and Raman scattering lidar can contribute to such aerosol characterization significantly since extinction coefficients can be measured independently from backscattering coefficients. In particular, HSRL can measure aerosol extinction during daytime and nighttime with a high sensitivity. We developed an HSRL with the iodine filter method for continuous observation of aerosols at 532nm in the northern region of Argentina in the framework of the South American Environmental Atmospheric Risk Management Network (SAVER.Net)/SATREPS project. The laser wavelength of the HSRL was controlled by a feedback system to tune the laser wavelength to the center of an iodine absorption line. The stability of the laser wavelength with the system satisfied the requirement showing very small systematic errors in the retrieval of extinction and backscatter.

Keywords: high spectral resolution lidar, Raman lidar, aerosol

1. INTRODUCTION

South America is a source of various aerosol types: biomass burning aerosols in the Amazon region [1], flying ashes from volcanic eruptions from the Andean Volcanic Belt [2], mineral dust from the Patagonian desert [3], and air pollution aerosols from urban areas [4,5]. Most of these aerosol species are detected in Argentina. Amazonian smoke is transported to the south eastern direction reaching Argentina from the northern frontier [6,7]. Volcanic ash from the June 2011 Puyehue-Cordón Caulle volcanic eruption was observed at Buenos Aires, Argentina [8,9] and caused severe air traffic disruptions in Argentina [10]. Continuous observation of temporal and spatial distribution of aerosols is very important to clarify effect of aerosols on the earth's climate and to provide hazard information for public health. Long-term observation of aerosol optical properties using sun photometers at the AErosol RObotic NETwork (AERONET) sites in Argentina has been performed [11], but the sun photometers cannot measure the aerosol vertical distribution that is needed for predicting the transport route of aerosols. Also, continuous observation with the sun photometers during nighttime is impossible.

In the past few years, an Argentinean Raman lidar network was constructed to continuously monitor the vertical distribution of volcanic ash and Patagonian dust [12,13]. From lidar data, extinction for aerosol components can be retrieved with various channels. Measuring depolarization ratios, non-spherical aerosols can be discriminated from spherical aerosols [14,15]. Using multi-wavelength information, fine and course particles can be discriminated [16]. Furthermore, high-spectral-resolution lidar (HSRL) and Raman lidar can measure extinction independently from backscatter, and the extinction-to-backscatter ratio (lidar ratio) is useful to determine absorbing aerosols [17]. Retrieval of extinction coefficients of black carbon with HSRL was demonstrated in [18].

HSRL measures spectrally-broadened Rayleigh scattering separately from spectrally narrower Mie scattering. Using Rayleigh and total (Mie + Rayleigh) scattering signals, aerosol extinction and backscattering can be retrieved without the assumption of the lidar ratio. Rayleigh scattering signals are sensitive enough to be measured during daytime and hence continuous observation of aerosols with HSRL is feasible. Recently, we developed an HSRL at the Lidar Division at the

Lidar Remote Sensing for Environmental Monitoring XV, edited by Upendra N. Singh, Nobuo Sugimoto, Achuthan Jayaraman, Mullapudi V. R. Seshasai, Proc. of SPIE Vol. 9879, 987912

Centro de Investigaciones en Láseres y Aplicaciones (CEILAP), in Buenos Aires, Argentina for long-term continuous observation of aerosol vertical distribution after being transported to the northern Argentinan region in the framework of South American Environmental Atmospheric Risk Management Network (SAVER.Net)/SATREPS Project [19]. This paper describes the HSRL system at the National Institute for Environmental Studies (NIES) in Japan as the basis of the measurement method, the development status of the HSRL at CEILAP, and the error analysis for retrieving aerosol extinction and backscatter.

2. HIGH SPECTRAL RESOLUTION AND RAMAN LIDAR SYSTEM IN NIES

Continuous observation of aerosols with a three-wavelength (1064 nm, 532 nm, and 355 nm) polarization-sensitive (532 nm and 355 nm) lidar is being performed at NIES, Tsukuba, Japan. The lidar has a high-spectral-resolution (HSR) optical element with an iodine absorption filter blocking the aerosol backscatter at 532 nm and a nitrogen Raman channel at 387 nm. The block diagram of the HSR and Raman lidar is shown in Figure 1.

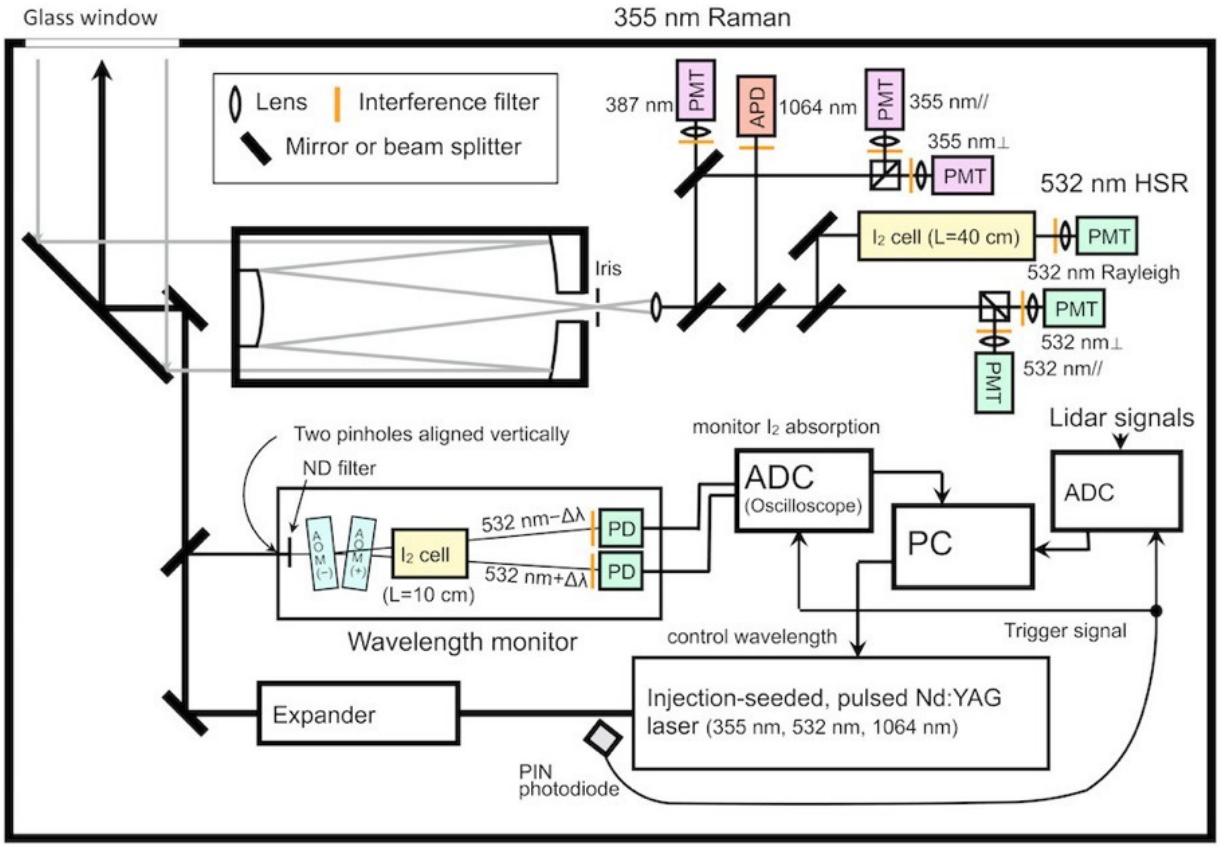

Figure 1. Block diagram of the three-wavelength Mie, high spectral resolution, and Raman lidar instruments in NIES [20].

A part of emission laser is sent into two acousto optic modulators (AOMs) to make both positive and negative Doppler-shifted diffracted beams. The two beams are measured with photo detectors after passing through a short iodine cell. Iodine absorption spectrum is obtained by scanning the laser wavelength, and then the laser wavelength is tuned to the center of the absorption line. The development of HSRL with iodine filters in NIES is described in [21] and the laser wavelength tuning system is briefly described in [22]. Figure 2 shows time-height intensity of range corrected signals for 1-month observation period. Stabilizing the laser wavelength, continuous observation with HSRL is achieved. Raman

signals are too noisy to retrieve extinction coefficient during daytime, but HSRL Rayleigh signals are available at daytime and nighttime.

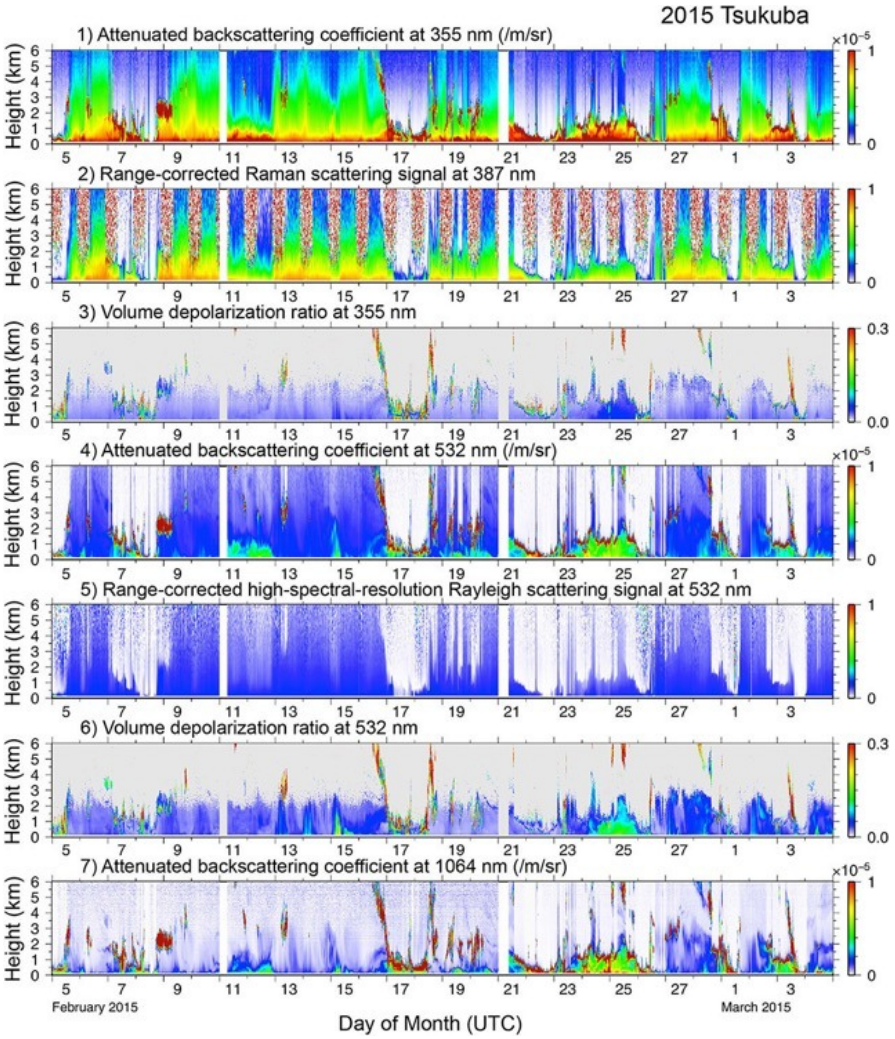

Figure 2. Observed data obtained from the NIES HSR and Raman lidar between 05 February 2015 and 04 March 2015 [20].

3. DEVELOPMENT OF HIGH SPECTRAL RESOLUTION LIDAR IN CEILAP

The new HSRL in Argentina was designed based on the multi-wavelength Raman lidar system of the Argentinian lidar network The laser wavelength locking system developed at NIES was attached to the emitter part. The HSRL design and test measurement results are reported by [23]. Here we describe the emitter system, the HSR receiver properties, and the laser wavelength stabilization with the laser wavelength feedback control system.

In the emitter part, the HSRL employs an injection-seeded single-mode Nd:YAG laser, Surelite II (Continuum, United States). The pulse repetition rate of the laser is 10Hz. The seed laser is a single-mode cw fiber laser consisted of a cavity with two fiber bragg gratings (FBG) in a Yb doped fiber. The output coupler FBG has narrow band reflectivity that allows single longitudinal mode oscillation. The laser wavelength is calibrated at the factory and can be tuned within a 20-30GHz range by changing the FBG heater temperature. To match a longitudinal mode of the host laser to the seeder laser wavelength, the cavity length of the host laser is determined to have the shortest build up time by controlling the piezo element mounted on the rear mirror of the host laser. The spectral width of output single longitudinal mode laser is $0.005cm^{-1}$.

In the receiver part, an iodine absorption filter is used as a HSR optical element to reject the Mie scattering and to penetrate part of Rayleigh scattering at the second harmonic wavelength (532 nm). The 1111 iodine absorption band in vacuum (18788.4510cm^{-1} [24]) is selected because of its strong absorption property. A pyrex glass cell (40 cm long, 5 cm inner diameter) enclosing iodine at low vacuum is set. The cell is wrapped in aluminum foil and a heating wire is further coiled to stabilize the temperature inside the cell. The cell temperature is monitored by a sensor and is set to be 50 ºC by a heat controller to achieve the strong absorption property of the Mie scattering. We measured the transmittance spectrum of the absorption line using the transmitter laser light. The minimum transmittance was 0.07 % and the full width at half maximum (FWHM) was 2.3 pm (Figure 3). The minimum transmittance is enough to block the Mie scattering light from aerosols and clouds and the FWHM can penetrate part of the Rayleigh scattering light. Calculated transmittance for Rayleigh scattering using the spectral shape is 28% at ground level.

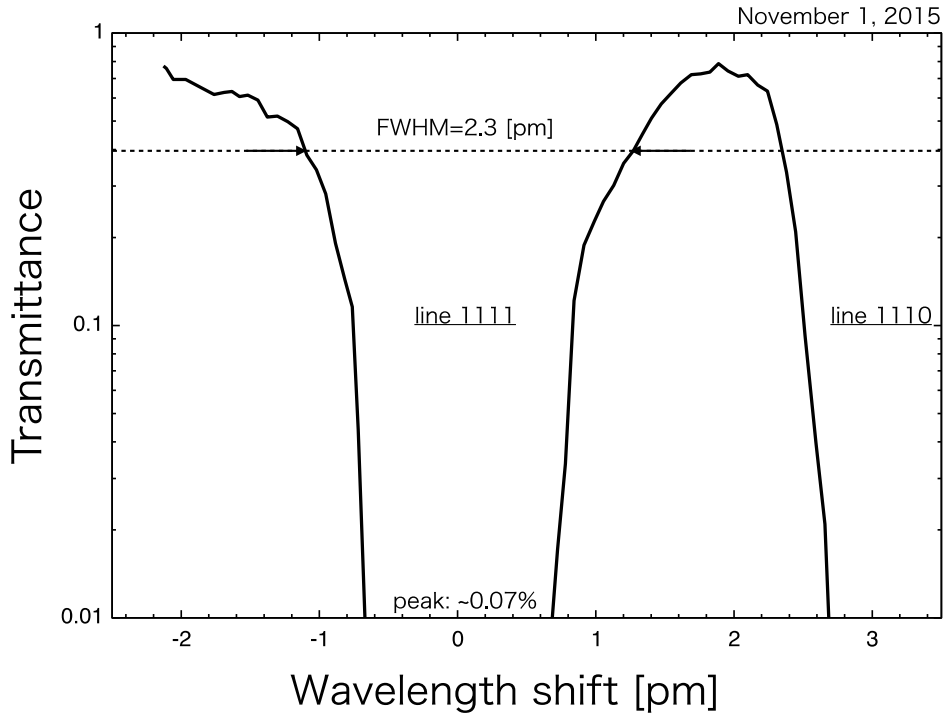

Figure 3. Transmittance spectrum of the iodine absorption filter (40 cm cell) used for the receiver part of the CEILAP HSRL.

To reject Mie scattering with the iodine filter, the laser wavelength must match the center of the 1111 iodine absorption line. In May 2015, a feedback control system was installed for stabilizing the laser wavelength for a long period of time since the laser wavelength may gradually change with time. A shorter iodine cell (20cm long) was set in the transmitter part and a beam partially reflected from the laser source is measured after passing through the cell for controlling the laser wavelength. The laser beam is reflected by an uncoated glass (15mm thickness) and is split into two beams. The two beams are then sent to the AOMs to make Doppler-shifted beams. The frequency shift is 0.25 pm (260 MHz) and the angle of the diffracted beam against the incident light is 33 mrad. Setting two AOMs in opposite direction, Stokes and Anti-Stokes light beams are generated. The two beams (positive and negative shifts) in addition to the unshifted beams are measured using photo detectors after passing through the 20 cm iodine cell and an interference filter.

Iodine absorption spectrum is obtained by scanning the laser wavelength and we can find the center of the iodine absorption line from the photodiode signals of the unshifted beam. The laser wavelength is then tuned to the center of the absorption line by using the signals of the Doppler-shifted beams. The laser wavelength is optimized by the gradient method: taking the ratio of the positively shifted signal (P+) to the negatively shifted signal (P-), the spectrum shape of the ratio (Prt = P+/P-) in logarithmic scale is similar to the first-order differentiation of the absorption spectrum (Figure 4(a)). Prt value at the center of the absorption line is used as the reference value, and thresholds from the reference value are set to stabilize the laser wavelength within 0.1 pm. If a certain Prt exceeds (falls below) the upper (lower) threshold, the heater temperature of the seed laser is turned down (up) by 0.035 pm to adjust the laser wavelength to the center of the absorption line. Standard deviation of the laser fluctuation resulted in 0.05 pm (54 MHz) (Figure 4(b)). The stability

of the laser wavelength is sufficient for retrieving aerosol extinction and backscatter with small systematic errors as discussed later.

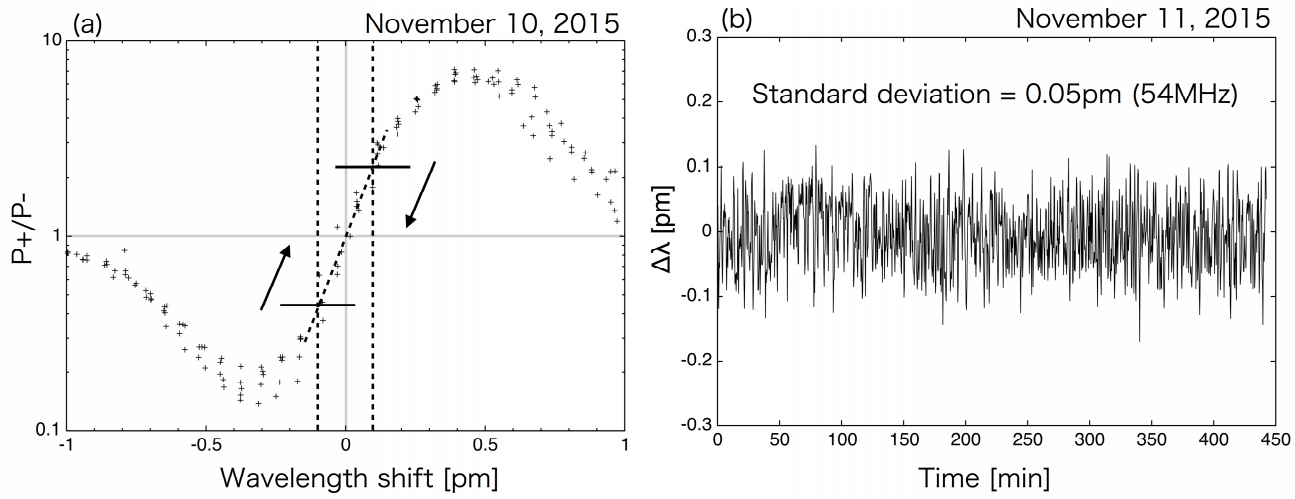

Figure 4. (a) Measured signal ratio P+/P- sweeping between ±1 pm wavelength shift from the center of the iodine absorption line. The vertical broken lines indicate the positions at ±0.1 pm wavelength shifts, the slanted broken line is the fitted line near the center, and the horizontal lines are the thresholds at ±0.1 pm wavelength shifts. The laser wavelength is tuned on the direction of the arrows if the measured P+/P- exceeds the thresholds. (b) Continuous monitoring of the laser wavelength fluctuation for the verification of the feedback control system.

4. ERROR ANALYSIS

In this section, we describe errors for the retrieval of extinction and backscatter from HSRL and Raman lidar data for the NIES and CEILAP lidars that have an HSR channel at 532 nm and a Raman channel at 387 nm. Ansmann et al., [25] discussed errors in detail for Raman lidar data analysis. The error sources of the Raman lidar analysis are the uncertainties of the wavelength dependence parameter and the temperature profile. Since the Raman wavelength is different from the laser wavelength, the wavelength dependence of the extinction has to be considered for the Raman lidar analysis. The wavelength dependence varies among aerosol types and it is an unknown parameter, but the errors in extinction are less than few percent. Uncertainty of temperature profiles causes errors in the calculation of molecular extinction and backscatter both for the HSRL and Raman lidar if the standard atmosphere is used. The errors are usually negligibly small and appear only in the case of strong inversion layers.

To calculate the aerosol backscatter by taking the signal ratio of elastic to Raman scattering channels, the attenuation term including the integral of the difference of elastic and Raman extinction coefficient from the lidar to the height of interest should be corrected. The extinction coefficients are unknown at lower heights where the geometric factor is less than 1, but the errors by the attenuation term correction are small. If the extinction coefficient is 0.1 /km (vertically constant) and the wavelength dependence is 1.0 (usually used for aerosols), the relative errors of backscatter at 1 km is –0.8 % for the uncorrected backscatter at 355 nm.

Systematic errors in HSRL arise from the uncertainty of transmittance of the iodine filter for Mie and Rayleigh scatterings. Uncertainty of transmittance for Mie (T_{Mie}) and Rayleigh (T_{Ray}) scatterings results from the deviation of the laser wavelength from the center of absorption line of iodine filter. The standard deviation of the laser wavelength fluctuation shown in Figure 4(b) leads to 3 % error in $\Delta T_{Mie}/T_{Mie}$ and 0.2 % error in $\Delta T_{Ray}/T_{Ray}$. T_{Ray} is much less sensitive to the laser wavelength deviation than T_{Mie}. The relative errors in backscatter by the uncertainty of transmittance are expressed as:

$$\frac{\delta\beta_1(r)}{\beta_1(r)} = -\frac{R(r)}{\beta_1(r)} \frac{\beta_1(r)\Delta T_{Mie} + \beta_2(r)\Delta T_{Ray}(r)}{T_{Ray}(r) - T_{Mie}}, \quad (1)$$

where β denotes the backscatter, R denotes the total-to-molecular backscattering ratio, and subscripts 1 and 2 are the Mie and Rayleigh scatterings, respectively. The relative errors in extinction by the uncertainty of the transmittance are expressed as:

$$\frac{\delta\alpha_1(r)}{\alpha_1(r)} = \frac{1}{2\alpha_1(r)\Delta r}\left[\frac{\delta X_{Ray}(r-\Delta r/2)}{X_{Ray}(r-\Delta r/2)} - \frac{\delta X_{Ray}(r+\Delta r/2)}{X_{Ray}(r+\Delta r/2)}\right], \tag{2}$$

where

$$\frac{\delta X_{Ray}(r)}{X_{Ray}(r)} = \frac{\beta_1(r)\Delta T_{Mie} + \beta_2(r)\Delta T_{Ray}(r)}{\beta_2(r)(T_{Ray}(r) - T_{Mie})}, \tag{3}$$

where Δr denotes the range interval for calculating the extinction. Estimated errors in extinction due to the uncertainty of transmittance are extremely small to be ignored. The relative errors in backscatter by ΔT_{Mie} are approximated by -7.5×10^{-5}R for the CEILAP HSRL and therefore they are negligible for aerosols. The relative errors in backscatter by ΔT_{Ray} decreases as R increases and are less than 1 % if R is greater than 1.3 for the CEILAP HSRL.

To reduce the retrieval errors in extinction, lidar signals should be averaged and smoothed to obtain better signal-to-noise ratio. If α_1 is 0.1 /km and Δr is 300 m, the required signal-to-noise ratio is 167 to have less than 10 % error in the extinction. We can get the signal-to-noise ratio from HSRL signals if the lidar signals are averaged over 5 ~ 15 minutes below 6 km. Compared to HSRL, Raman lidar has worse signal-to-noise ratio, and therefore we have to integrate the signals over 30 minutes to ~ 2 hours to achieve less than 10 % of the retrieval errors. As pointed out in Ansmann et al., [25], averaging over a long period of time can cause large errors up to several tens of percent for non-uniform layers.

Random errors in the backscatter retrieval are determined by the total-to-molecular backscattering ratio (R) and the signal-to-noise ratios. If R is 2, the required signal-to-noise ratio is 20 for a 10 % error in the backscatter, and hence the random errors in the backscatter are much less than those in the extinction for a certain signal-to-noise ratio. In the backscatter retrieval, the signal ratio between the total (elastic) and the Rayleigh (Raman) channels should be calibrated at the height where aerosols and clouds are free. Due to the low signal-to-noise ratio at the reference height, the calibration coefficient suffers from random errors that would be dominant in the retrieval error of backscatter. Rather than calculating signal ratios at the reference height for every averaged profile, the calibration coefficient should be beforehand calculated by averaging the signals over a long time, enough to neglect random errors in clear sky condition days. The calibration coefficient may contain systematic errors for Raman lidar due to the wavelength dependence of the extinction coefficient, but the errors are negligible for clear days.

5. CONCLUSION

We developed an HSRL using the iodine absorption filter method at CEILAP, Argentina. The HSRL was built based on the multi-wavelength Raman lidar of the Argentinean lidar network and the HSRL system developed at NIES, Japan. For long-term aerosol observation with the HSRL, a feedback control system was installed for automatically tuning the laser wavelength to the center of the iodine absorption line. The standard deviation of the laser wavelength fluctuation with the system was ±0.05 pm from the center of the absorption line. With the stability, the system can retrieve extinction and backscatter with small systematic errors. We conducted a test measurement with the HSRL and confirmed favorable results as reported by [23]. We plan to deploy the developed HSRL to the northern region of Argentina in the near future. Continuous monitoring of black carbon from the Amazonian region and other aerosols with the HSRL is expected.

ACKNOWLEDGMENTS

This research was supported by Science and Technology Research Partnership for Sustainable Development (SATREPS), Japan Science and Technology Agency (JST)/Japan International Cooperation Agency (JICA).

REFERENCES

[1] Brito J., Rizzo L. V., Morgan W. T., Coe H., Johnson B., Haywood J., Longo K., Freitas S., Andreae M. O., and Artaxo P., "Ground-based aerosol characterization during the South American Biomass Burning Analysis (SAMBBA) field experiment," Atmos. Chem. Phys. 14, 12069-12083 (2014).

[2] Carn S. A., Pallister J. S., Lara L., Ewert J. W., Watt S., Prata A. J., Thomas R. J., and Villarosa G., "The unexpected awakening of Chaitén volcano, Chile," Eos 90(24), (2009).

[3] Gassó S., and Stein A. F., "Does dust from Patagonia reach the sub-Antarctic Atlantic Ocean?," Geophys. Res. Lett. 34, L01801 (2007).

[4] Miranda R. M., Andrade M. F., Fornaro A., Astolfo R., Andre P. A., Saldiva P., "Urban air pollution: a representative survey of PM2.5 mass concentrations in six Brazilian cities," Air Qual. Atmos. Health 5, 63-77 (2012).

[5] Muñoz R. C., and Alcafuz R. I., "Variability of urban aerosols over Santiagom Chile: comparison of surface PM10 concentrations and remote sensing with ceilometer and lidar," Aerosol Air Qual. Res. 12, 8-19 (2012).

[6] Longo K., Freitas S., Ulke A. G., and Hierro R. F., "Transport of biomass burning products in southeastern South America and its relationship with the south american low level jet east of the Andes," Proc. 8 ICSHMO, 121-129 (2006).

[7] Otero L. A., Ristori P. R., Holben B., and Quel E. J., "Detection of biomass burning aerosols in Córdoba, Argentina, using the AERONET / NASA data base," Óptica Pura y Aplicada 37(3), 3359-3363 (2004).

[8] Otero L. A., Ristori P. R., Pallotta J. V., Pawelko E. E., and Quel E. J., "The Puyehue-Cordón Caulle volcanic eruption, June 2011: water vapor, atmospheric boundary layer and aerosol temporal evolution in Buenos Aires, Argentina," Revista Boliviana de Física 21, 27-29 (2012).

[9] Ristori P. R., Otero L. A., Pallotta J. V., Pawelko E. E., and Quel E. J., "Biomass burning and volcanic ash characterization at Centro de Investigaciones en Láseres y Aplicaciones, Buenos Aires, Argentina," Revista Boliviana de Física 21, 30-32 (2012).

[10] Wilson T., Stewart C., Bickerton H., Baxter P., Outes V., Villarosa G., Rovere E., "Impact of the June 2011 Puyehue-Cordón Caulle volcanic complex eruption on urban infrastructure, agriculture and public health," GNS Science Report 2012/20, (2013).

[11] Olcese L., Palancar G. G., and Toselli B. M., "Aerosol optical properties in central Argentina," J. Aerosol Sci. 68, 25-37 (2014).

[12] Ristori P. R., Otero L. A., Pawelko E., Pallota J., D'Elía R., Chouza F., Gonzalez F., Dworniczak J. C., Vilar O., Pereyra A., Fernández M., Lema S., Sugimoto N., Quel E. J., "Development of an Argentinean lidar network to monitor the volcanic plume and dust in Patagonia," Proc. 26th International Laser Radar Conference, 357-360 (2012).

[13] Chouza F., Dworniczak C. D., Otero L., Pallotta J., Proyetti M., Quel E., Ristori P., Sugimoto N., Vilar O., and Wolfram E., "Monitoring volcanic ash in the atmosphere," SPIE Newsroom, Jun. 17 2013.

[14] Sugimoto N., Matsui I., Shimizu A., Uno I., Asai K., Endoh T., Nakajima T., "Observation of dust and anthropogenic aerosol plumes in the Northwest Pacific with a two-wavelength polarization lidar on board the research vessel Mirai," Geophys. Res. Lett. 29(19), 1901 (2002).

[15] Shimizu A., Sugimoto N., Matsui I., Arao K., Uno I., Murayama T., Kagawa N., Aoki K., Uchiyama A., and Yamazaki A., "Continuous observation of Asian dust and other aerosols by polarization lidars in China and Japan during ACE-Asia," J. Geophys. Res. 109, D19S17 (2004).

[16] Nishizawa T., Okamoto H., Sugimoto N., Matsui I., Shimizu A., and Aoki K., "An algorithm that retrieves aerosol properties from dual-wavelength polarization lidar measurements," J. Geophys. Res. 112, D06212 (2007).

[17] Burton S. P., Ferrare R. A., Hostetler C. A., Hair J. W., Rogers R. R., Obland M. D., Butler C. F., Cook A. L., Harper D. B., and Froyd K. D., "Aerosol classification using airborne High Spectral Resolution Lidar measurements – methodology and example," Atmos. Meas. Tech. 5, 73-98 (2012).

[18] Nishizawa T., Sugimoto N., Matsui I., Shimizu A., Tatarov B., and Okamoto H., "Algorithm to retrieve aerosol optical properties from high-spectral resolution lidar and polarization Mie-scattering lidar measurements," IEEE Trans. Geosci. Rem. Sens. 46(12), 4094-4103 (2008).

[19] Quel E., Sugimoto N., Otero L., Jin Y., Ristori P., Nishizawa T., González F., Papandrea S., Shimizu A., and Mizuno A., "Aerosols monitoring network to create a volcanic ash risk managements system in Argentina and Chile," Proc. 27th International Laser Radar Conference, S9-06 (2015).
[20] Sugimoto N., Nishizawa T., Shimizu A., Matsui I., Jin Y., Higurashi A., Uno I., Hara Y., Yumimoto K., and Kudo R., "Continuous observation of atmospheric aerosols across East Asia," SPIE Newsroom, Oct. 21 2015.
[21] Liu Z., Matsui I., Sugimoto N., "High-spectral resolution lidar using an iodine absorption filter for atmospheric measurements," Opt. Eng. 38(10), 1661-1670 (1999).
[22] Nishizawa T., Sugimoto N., and Matsui I., "Development of a dual-wavelength high-spectral-resolution lidar," Proc. SPIE, 7860 (2010).
[23] Papandrea S., Jin Y., Ristori P., Otero L., Nishizawa T., Mizuno A., Sugimoto N., and Quel E., "Construction and first atmospheric observation of a high spectral resolution lidar system in Argentina in the frame of a trinational Japanese-Argentinean-Chilean collaboration," Proc. SPIE, submitted, (2016).
[24] Gerstenkorn S., and Luc P., "Atlas du spectre d'absorption de las molecule d'iode," Center National de las Recherche Scientifique, Paris, (1978).
[25] Ansmann A., Wandinger U., Riebesell M., Weitkamp C., and Michaelis W., "Independent measurement of extinction and backscatter profiles in cirrus clouds by using a combined Raman elastic-backscatter lidar," Appl. Opt. 31(33), 7113-7131 (1992).